

Neural control exploits changing mechanical advantage and context dependence to generate different feeding responses in *Aplysia*

Gregory P. Sutton¹, Elizabeth V. Mangan¹, David M. Neustadter^{2,3}, Randall D. Beer⁴, Patrick E. Crago², Hillel J. Chiel^{2,5}

¹ Case Western Reserve University, Department of Mechanical and Aerospace Engineering, Cleveland OH, USA

² Case Western Reserve University, Department of Biomedical Engineering, Cleveland OH, USA

³ Current address: Elbit Systems Ltd., Haifa, Israel, 31053

⁴ Case Western Reserve University, Department of Electrical Engineering and Computer Science, Cleveland OH, USA

⁵ Case Western Reserve University, Departments of Biology and Neurosciences, 2080 Adelbert Road, Cleveland OH, 44106-7080, USA

Received: 26 April 2004 / Accepted: 5 August 2004 / Published online: 27 October 2004

Abstract. How does neural control reflect changes in mechanical advantage and muscle function? In the *Aplysia* feeding system a protractor muscle's mechanical advantage decreases as it moves the structure that grasps food (the radula/odontophore) in an anterior direction. In contrast, as the radula/odontophore is moved forward, the jaw musculature's mechanical advantage shifts so that it may act to assist forward movement of the radula/odontophore instead of pushing it posteriorly. To test whether the jaw musculature's context-dependent function can compensate for the falling mechanical advantage of the protractor muscle, we created a kinetic model of *Aplysia*'s feeding apparatus. During biting, the model predicts that the reduction of the force in the protractor muscle I2 will prevent it from overcoming passive forces that resist the large anterior radula/odontophore displacements observed during biting. To produce protractions of the magnitude observed during biting behaviors, the nervous system could increase I2's contractile strength by neuromodulating I2, or it could recruit the I1/I3 jaw muscle complex. Driving the kinetic model with in vivo EMG and ENG predicts that, during biting, early activation of the context-dependent jaw muscle I1/I3 may assist in moving the radula/odontophore anteriorly during the final phase of protraction. In contrast, during swallowing, later activation of I1/I3 causes it to act purely as a retractor. Shifting the timing of onset of I1/I3 activation allows the nervous system to use a mechanical equilibrium point that allows I1/I3 to act as a protractor rather than an equilibrium point that allows I1/I3 to act as a retractor. This use of equilibrium points may be similar to that proposed for vertebrate control of movement.

1 Introduction

Although it is a common assumption in biomechanical models that the mechanical advantage of muscles

remains constant during behaviors (Taga 1995; Ijspeert 2001; Kaske et al. 2003), the mechanical advantage and the function of muscles may change throughout behavior, and neural control must reflect these changes (Zajac 1993). In many animals, as muscle contracts, its mechanical advantage decreases so that the muscle becomes less able to generate force. For example, during tentacle extension, the transverse muscles in the squid lose mechanical advantage and become less able to extend the tentacle (Van Leeuwen and Kier 1997). This is also the case for transverse muscles during tongue extensions of the pig-nosed frog (Van Leeuwen et al. 2000) and the lizard (Chiel et al. 1992). In humans, as the hip extends, the mechanical advantage of many of the hip extensors decreases, with the hamstrings' mechanical advantage dropping precipitously at large hip extensions (Hoy et al. 1990). Similar decrements are seen in hip extensors and flexors in the frog (Kargo and Rome 2002).

Neural control must also adapt to changes in muscle function as the geometry of a muscle's surrounding structures changes. In the human shoulder, changes in limb position can change the anterior deltoid's function from adduction to flexion or reverse the function of the pectoralis from flexion to extension (Buneo et al. 1997; Yoshida et al. 2002). In the leg, gluteus medius and gluteus minimus can also reverse their function from hip flexion to hip extension as a function of joint position (Hoy et al. 1990). In the frog leg, the cruralis, gracilis, adductor magnus, and iliofibularis all change their behavioral function depending on joint position (Kargo and Rome 2002). The functions of these muscles, as defined by the direction of the forces and torques they exert, are context dependent. Changes in mechanical advantage and function are both constraints and opportunities for neural control.

To understand how neural control effectively responds to changes in mechanical advantage and muscle function, it would be useful to combine a kinetic model of the biomechanics with information about the neural control (Zajac 1993). Deducing general principles from kinetic models about neural control is often difficult because of lack of appropriate data about the nervous system (Zajac 1993;

Correspondence to: H. J. Chiel
(e-mail: hjc@po.cwru.edu,
Tel.: +1-216-3683846, Fax: +1-216-3684672)

Koike and Kawato 1995; Alfaro and Herrel 2001; Zajac et al. 2002). While EMG is often used as a correlate of motor neuron activity, the relationship between EMG and motor neuron activity is approximate (Zajac 1993). Furthermore, this relationship can be changed by both extrinsic and intrinsic neuromodulation (Belanger and Orchard 1993; Brezina et al. 2000b; Hurwitz et al. 2000). One way to understand how neural control responds to biomechanical changes during behavior is to build kinetic models of animal behaviors that are accompanied by detailed information about the neuronal basis of these behaviors.

The feeding structure (the buccal mass) of the marine mollusc *Aplysia californica* is an ideal system for studying neural control and changes in biomechanics because much is known about both. Within the ganglia that control feeding behaviors, motor neurons (Lotshaw and Lloyd 1990; Church et al. 1991; Morton and Chiel 1993a,b; Church and Lloyd 1994; Evans et al. 1996), interneurons (Hurwitz et al. 1997; Evans and Cropper 1998; Jing and Weiss 2001, 2002; Jing et al. 2003), and sensory neurons (Miller et al. 1994; Evans and Cropper 1998; Rosen et al. 1982, 2000a,b) have been identified and characterized. In vivo EMG and ENG have been recorded from the animal during feeding behaviors, and the activity observed in these recordings has been correlated with activity from individual identified neurons (Morton and Chiel 1993a,b; Hurwitz et al. 1996). In addition, within the musculature of the buccal mass, changes in mechanical advantage and context dependence are observed: the I2 muscle loses mechanical advantage as it contracts, and the I1/I3/jaw muscle complex may have context-dependent effects (Chiel et al. 2003). Models exist for buccal mass muscles (Yu et al. 1999; Brezina et al. 2000a), and both data and models have been used to investigate the roles of neuromodulation in changing muscles' response to neural activation (Brezina et al. 2000b; Hurwitz et al. 2000). As a consequence, it is possible to develop hypotheses about how neural control interacts with biomechanical changes during feeding.

The nervous system of *Aplysia* generates several qualitatively different feeding responses in which the mechanical advantage and function of the musculature change. Two of *Aplysia's* ingestive feeding behaviors, biting and swallowing, can be differentiated by the amount of extension (protraction) of the grasping structure (the radula/odontophore) toward the jaws (Kupfermann 1974): there is less protraction in swallowing than in biting. During both behaviors, protraction is initiated by contraction of I2 (Hurwitz et al. 1996) and resisted by the passive forces of the hinge (Sutton et al. 2004). At the peak of protraction in biting the passive hinge forces are very large compared to the force that I2 can apply (Sutton et al. 2004) because I2 shortens, reducing its mechanical advantage and its force (Yu et al. 1999). This leads to the hypothesis that protractor muscle I2 may not be able to generate a biting protraction without assistance. The nervous system could use neuromodulation to enhance I2's contractile strength (Hurwitz et al. 2000) and/or cocontract a context-dependent muscle, I1/I3 (Chiel et al. 2003). During swallows, I1/I3 receives neural activation only after full protraction of the radula/odontophore. In contrast,

during bites, the timing of onset of I1/I3 activation shifts so that I1/I3 begins to receive neural input during the protraction phase (Hurwitz et al. 1996), suggesting that, during bites, I1/I3 may assist I2 in protraction of the radula/odontophore.

To test the hypothesis that the change in phase of activation of I1/I3 relative to I2 could play a role in generating the strong protractions of biting, we built a kinetic model of the buccal mass of *Aplysia* that includes I2, the posterior portion of the I3, the passive forces that resist I2, and the radula/odontophore. We compared the force that I2 could apply to protract the radula/odontophore with the passive forces that resist protraction. We also used the model with in vivo EMG and ENG as input to determine if the shift in activation in the posterior part of I3 is sufficient to generate the protractions seen in biting. Our results suggest that the phase shift in activation of the posterior part of I3 between in vivo biting and swallowing behaviors is a specific example of neural control shifting the equilibrium positions of the radula/odontophore to generate biting or swallowing behaviors. The nervous system controlling the musculature's equilibrium positions is a control strategy that has also been suggested for vertebrates (Bizzi et al. 1992; Flash and Sejnowski 2001).

2 Materials and methods

2.1 Anatomy of the *Aplysia* buccal mass

Aplysia californica is a generalist herbivore that feeds on seaweed. The *Aplysia* feeding apparatus is known as the buccal mass. The animal grasps seaweed with a pincer-like structure, the radula/odontophore. During feeding, the radula/odontophore is translated and rotated anteriorly toward the jaws (i.e., it is *protracted*), it grasps food, and then it translates and rotates posteriorly (i.e., it is *retracted*) to deposit food in the esophagus (Fig. 1a shows a schematic diagram of the anatomy; Fig. 1c schematically represents movements during biting). Posterior to the radula/odontophore is a thin sheet of muscle, the I2 (nomenclature from Howells 1942). Anterior to the radula/odontophore is the I1/I3/jaw muscle complex (Fig. 1a), which is innervated by buccal nerve 2 (BN2). The radula/odontophore is attached to the other muscles at a ventral interdigitation point, known as the hinge, which is composed of the fibers of the I2 muscle, the I3 muscle complex, and the largest radula/odontophore muscle, I4 (Drushel et al. 1997). On the dorsal side of the radula/odontophore is a cylindrical mass of cartilaginous tissue called the radular stalk.

2.2 Magnetic resonance measurements of radula/odontophore kinematics

To measure in vivo radula/odontophore shape during biting, we obtained magnetic resonance (MR) images of bites (acquisition rate of 3 Hz) of intact behaving animals using

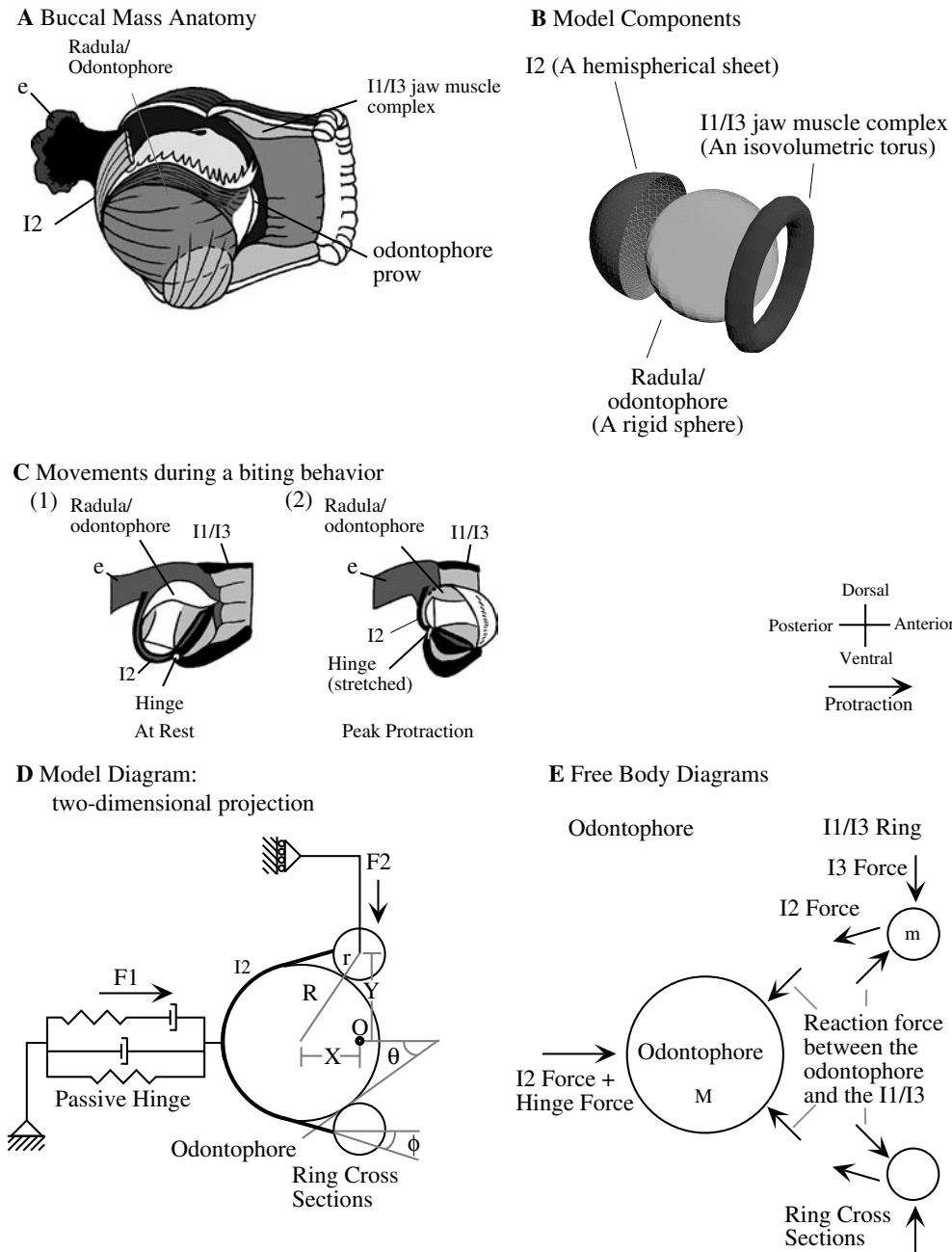


Fig. 1a–e. Buccal mass anatomy and the kinetic model. **a** Anatomical drawing of the buccal mass at rest, with landmarks labeled and part of the tissue dissected away to show the internal structures. The schematic drawing is by Dr. Richard F. Drushel. **b** Three-dimensional representation of the model’s components. The radula/odontophore is represented by a rigid sphere, the I1/I3 by a torus, and the I2 by a hemispherical sheet that attaches to I1/I3. **c** Buccal mass movements during a biting behavior. During a biting behavior, the buccal mass starts at rest (1), the radula/odontophore rolls and translates toward the jaws (protraction, 2), and then the radula/odontophore returns to rest (back to position 1). Note that the I2 muscle shortens significantly

at the peak protraction of biting, and that part of the I3 muscle is posterior to the midline of the radula/odontophore. **d** A 2-D cut-through of the model. The variables that define the model’s state are labeled in the figure. F_1 is the sum of all the horizontal forces on the radula/odontophore; F_2 is the sum of all the vertical forces on the radula/odontophore. The contraction of I1/I3 gives rise to a force in the plane of the I1/I3 that acts on the radula/odontophore (F_2). The resultant horizontal force on the radula/odontophore is the component out of the plane defined by the I1/I3 ring of the reaction force [$F_2 \tan(\theta)$], which lies along the X axis of the figure. **e** Free-body diagrams of the individual model pieces

methods described in Neustadter et al. (2002). Two behaviors from two animals were sufficiently free of parallax to be analyzed. Radula/odontophore eccentricity was measured by defining two axes on the radula/odontophore, one parallel to the radular stalk, and one

perpendicular to the radular stalk. Radula/odontophore eccentricity is the ratio of the radula/odontophore length parallel to the stalk to the radula/odontophore length perpendicular to the stalk.

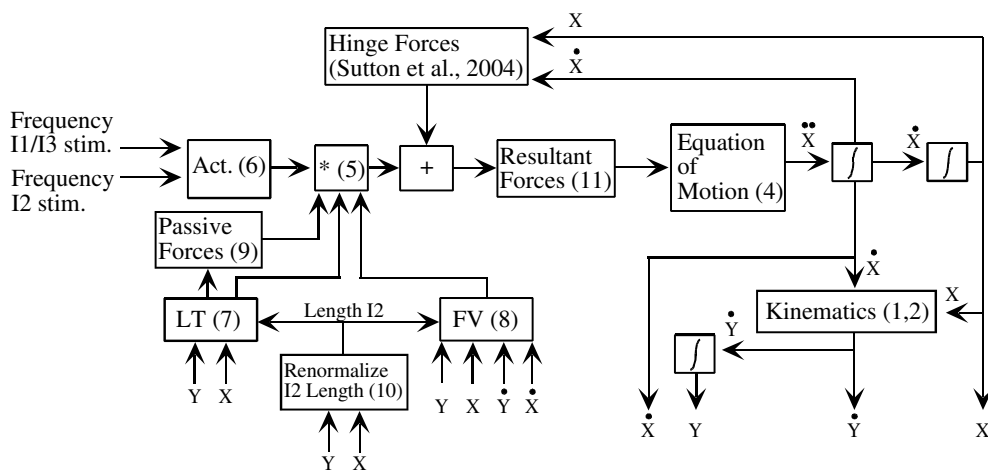


Fig. 2. Flow diagram of the model's calculations. The equations for each component are listed in the text by equation number. The model uses the current geometry and muscle activations to calculate muscle forces and radula/odontophore acceleration and then inte-

grates acceleration to calculate radula/odontophore position. The I1/I3 velocity is solved from the model's geometry and then integrated to calculate I1/I3 torus position. The I1/I3 radius, r , is calculated from the geometry. *Act* activation, *LT* length/tension, *FV* force/velocity

2.3 Model overview

Frequencies of stimulation for I1/I3 and I2 were input to the model, which returned the radula/odontophore displacement as output. The model passed muscle stimulation frequencies through a first-order low-pass filter (Yu et al. 1999) to represent muscle activation, which drove a Hill-type muscle model. The muscle model calculated individual muscle tensions, which were used to calculate the forces on the radula/odontophore. The muscle forces were input to the system's equation of motion to calculate radula/odontophore acceleration. The accelerations and velocities were then integrated to yield the positions (a flow diagram of the model is shown in Fig. 2).

2.4 Model components

The kinetic model was made up of four components: a radula/odontophore, an I1/I3, an I2, and a model of the passive hinge forces (the first three are shown schematically in Fig. 1b). The radula/odontophore was modeled as a sphere that was free to move only in the anterior/posterior direction (the X direction). The I1/I3 was modeled as a torus that was free to open or close along its major radius but constrained to be isovolumetric (Abbott and Baskin 1962) and to maintain contact with the radula/odontophore. This was a simplification of the anatomy of the I1/I3 jaw complex but provided a reasonable initial model of its posterior portion. The I2 was modeled as a sheet posterior to the radula/odontophore that attached to the I1/I3. The anatomical hinge (Fig. 1c) was modeled with a Kelvin and a Maxwell viscoelastic element in parallel (Fig. 1d) that captured the translational component of the anatomical hinge and was identical to the model presented in Sutton et al. (2004).

The assumption that the radula/odontophore was a sphere, while not appropriate to characterize an entire feeding response, was appropriate to characterize

protractions during biting and swallowing. During these behaviors, the in vivo radula/odontophore was spherical during peak protraction [Fig. 3; eccentricity in biting = 1.1 ± 0.1 ($N = 2$); eccentricity in swallowing = 1.2 ± 0.1 (Neustadter et al. 2002; $N = 4$, Fig. 12)] and then adopted an ellipsoidal shape during the retraction phase (Drushel et al. 1997; Neustadter et al. 2002). Because the radula/odontophore was spherical during protraction, the model's assumptions about radula/odontophore shape were adequate to make predictions about protraction movements. During the protraction phase in egestive behaviors, however, the radula/odontophore's shape might have differed because it was closed rather than opened, so predictions that the kinetic model made about biting and swallowing may not be applicable to egestive behaviors.

2.5 The model's governing equation of motion

The model's governing equation of motion was derived from three equations. The first two equations were the kinematic constraint equations: the I1/I3 torus must both remain in contact with the spherical radula/odontophore and be isovolumetric. For the torus and sphere to be in contact, the distances X and Y must form a right triangle with a hypotenuse of length $(R + r)$ (geometric variables labeled in Fig. 1d).

Torus and sphere must be in contact:

$$X^2 + Y^2 = (R + r)^2. \quad (1)$$

For the torus to be isovolumetric, the radius, r , of the torus must decrease as the major axis of the torus, Y , increases, and vice versa, so that the volume is constant.

Isovolumetric torus constraint:

$$2\pi^2 r^2 Y = V_{I1I3}, \quad (2)$$

where V_{I1I3} is a constant volume. The third equation was the application of Newton's second law to solve for

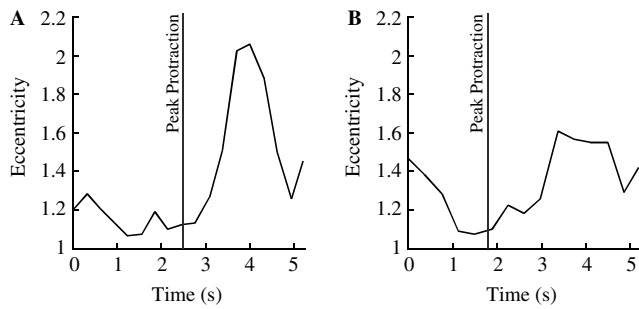


Fig. 3a,b. Magnetic resonance imaging measurements of midsagittal radula/odontophore eccentricity during biting in vivo from two behaviors (**a**: sequence 3213, frames 26–43, **b** sequence 3222, frames 611–625). Two axes were determined, one parallel to the radular stalk and one perpendicular to it. The ratio of the length of the parallel axis to the length of the perpendicular axis defined the eccentricity of the midsagittal cross section of the radula/odontophore. During the protractions of both bites the radula/odontophore's shape was very close to a circle (eccentricity was close to 1.0). As the radula/odontophore retracted, however, its shape changed from being circular to being more ellipsoidal. Because the model assumed the radula/odontophore was a sphere, model conclusions that depended on shape were accurate only during the protraction phase of biting. During the retraction phase, the model was less accurate because of its incorrect assumption of a spherical radula/odontophore shape

the relationship between radula/odontophore acceleration (\ddot{X}), I1/I3 acceleration (\ddot{Y}), the angle between them (θ), and the forces within the system (F_1 , F_2) (free-body diagrams are shown in Fig. 1e):

Newton's second law:

$$(m\ddot{Y} + F_2) \cos(\theta) = (M\ddot{X} - F_1) \sin(\theta), \quad (3)$$

where M is the mass of the radula/odontophore and m is the mass of the I1/I3. While inertial forces within the model were small, inclusion of mass simplified implementation of the model. This model, however, was insensitive to changes in radula/odontophore or I1/I3 mass (data not shown).

Equations (1)–(3) were solved for the radula/odontophore acceleration. The resulting equation of motion (EOM) of the system is

$$\ddot{X} = \frac{m \tan(\theta)((2\dot{Y}\dot{X}X + 2Y\dot{X}^2 + 4Y\dot{Y}^2 + r\dot{Y}\dot{r} + (R+r)\dot{r}\dot{Y}) + F_2(-2Y^2 - (R+r)r) - F_1(-2Y^2 - (R+r)r)}{(-2Y^2 - (R+r)r)M - 2YXm \tan(\theta)}. \quad (4)$$

2.6 The Muscle model

Tension in I2 and I3 (T_{I2} and $T_{I1/I3}$) were modeled with tendonless Hill-type muscle models with nonlinear activation dynamics, following the model developed by Yu et al. (1999)¹ [notation consistent with Yu et al. (1999)]:

¹ The muscle model parameters are shown in Table 1. The g parameter used in Yu et al. (1999) was for normalization purposes only and was not needed for this formulation of the activation function. Based on the examination of other datasets, the F_o in Yu et al. (1999) may not have been typical of the population. We therefore set a higher F_o for I2. There is a sign difference between the Yu et al. (1999) force-velocity lengthening equation and the one presented here; the former contained a sign error (P.E. Crago, personal communication).

$$\text{Muscle Tension} = F_o(\text{Act}(t)LT[L_m(t)]FV[V_m(t)] + \text{Passive Tension}[L_m(t)]). \quad (5)$$

To model the muscles' excitation by the temporal summation of excitatory junction potentials, we defined an activation function [$\text{Act}(t)$] for each muscle using three equations:

$$u(t) = A - Be^{-C*\text{freq}(t)} \quad -0.3 \leq u(t), \quad (6a)$$

$$\frac{da(t)}{dt} = \tau^{-1}\{u(t) - [\beta + (1-\beta)u(t)]a(t)\} \quad -a_o \leq a(t), \quad (6b)$$

$$\text{Act}(t) = a(t) - a_o \quad 0 \leq \text{Act}(t) \leq 1, \quad (6c)$$

with $\text{freq}(t)$ being the frequency of activation of the muscle.

The length-tension property for both muscles was assumed to be the length tension property developed by Yu et al. (1999) and was a function of L_m (muscle length) and L_{opt} (optimal muscle length):

$$LT[L_m] = G_1 - G_2 \frac{L_m}{L_{opt}} + G_3 \frac{L_m^2}{L_{opt}^2} - G_4 \frac{L_m^3}{L_{opt}^3}. \quad (7)$$

Both muscles' force-velocity properties were also assumed to be identical and were represented by two equations, one for lengthening (defined as negative muscle velocities, $V_m < 0$) and one for shortening (defined as positive muscle velocities, $V_m > 0$):

$$FV \text{ lengthening} = 1 + \frac{H_1}{1 - L_{opt}H_2/V_m}, \quad (8a)$$

$$FV \text{ shortening} = \frac{1}{1 + V_m H_3/L_{opt}}. \quad (8b)$$

The passive tension in each muscle was parameterized identically as in Yu et al. (1999):

$$\text{Passive Muscle Tension} = J_1 + J_2 e^{(L_m/L_{opt} - J_3)/J_4}. \quad (9)$$

To map the geometric length changes of I2 to the in vivo length changes, we transformed the I2 length to ensure that the model I2's length-tension curve was similar

to that observed in vivo. The linear transformation was constrained by the rest and minimum length values of I2 observed in vivo in Fig. 12 of Drushel et al. (1998).

$$\text{renormalized_I2_length} = K_1 \text{model_I2_length} + K_2 \quad (10)$$

The model I3 was given a smaller B parameter, which decreased the model I1/I3's latency of response to 0.5 s, so that the model would match I1/I3's minimum in vitro latency of 0.5 s (Fox and Lloyd 1997) (Table 1). At this value, the model I3 had a threshold stimulation frequency of 5 Hz. Below 5 Hz, the simulated I3 decayed with a time constant of 2.45 s in order to allow I3 to relax as quickly as an unstimulated I2.

Table 1. Parameter values

Parameter name	Value
a_0	1.65×10^{-1}
A	1.03
B_{I2}	4.31
B_{I1I3}	1.0
C	-1.98×10^{-2}
β	4.96×10^{-1}
τ	2.45(s)
G_1	1.81
G_2	1.08×10^1
G_3	1.92×10^1
G_4	9.2
H_1	6.1×10^{-1}
H_2	3.8×10^{-2}
H_3	1.08×10^1
J_1	-4.1×10^{-1}
J_2	1.04
J_3	1.18
J_4	2.8×10^{-1}
F_{oI2}	2.4×10^{-1} (N)
F_{oI3}	7.2×10^{-1} (N)
M	1.7×10^{-3} (kg)
m	1.3×10^{-3} (kg)
Radula/odontophore radius	5×10^{-3} (m)
V_{I1I3}	1.2×10^{-7} (m ³)
K_1	5.9×10^{-1}
K_2	3.5×10^{-1}
L_{I2opt}	2.25×10^{-2} (m)
$L_{I1I3opt}$	4.0×10^{-2} (m)
I2 EMG scaling factor	7.0
Hinge parameters (from Sutton et al. 2004)	
A_1	6.2×10^{-3} (N/m)
A_2	2.4×10^1 (N/m)
X_o	1.3×10^{-2} (m)
D_x	2.4×10^{-3} (m)
B_1	-5.87×10^1 (N/m)
B_2	1.26×10^4 (N/m ²)
B_3	-9.0×10^5 (N/m ³)
B_4	2.4×10^7 (N/m ⁴)
C_1	-9.0×10^{-3} (N/m)
C_2	2.7×10^2 (N/m ²)
C_3	1.0×10^5 (N/m ³)
D_1	-1.6 (N/m)
D_2	5.4×10^2 (N/m ²)
E_1	4.0 (N s/m)
F_1	1.1×10^1 (N s/m)
F_2	-8.2×10^2 (N s/m ²)
F_3	1.7×10^6 (N s/m ³)
G_{1Hinge}	-2.0×10^1 (N s/m)
G_{2Hinge}	-8.6×10^2 (N s/m ²)

2.7 Muscle forces on the radula/odontophore

In order to calculate the resultant forces on the radula/odontophore (F_1 and F_2) from muscle tension (T_{I2} and

Fig. 4. Mechanical analysis of I2's maximum force on the radula/odontophore as a function of BMLs of radula/odontophore displacement. This force is a function of I2's length-tension property (**a**) and I2's mechanical advantage (**b**). I2's mechanical advantage is defined by the ratio of I2 tension to the force that I2 applies to the radula/odontophore (equation 11a,b). As the radula/odontophore protracts (displaces anteriorly from rest), I2's length-tension (**a**) and mechanical advantage (**b**) decrease. The rise in the mechanical advantage at large protractions occurs because after the radula/odontophore midline passes the I1/I3, contraction of I2 will close the I1/I3 behind the odontophore [in the cross-sectional sketch marked "Prot.", contraction of the I2 (*bold line*) will bring the top of the I1/I3 and the bottom of the I1/I3 closer together]. **c** The maximum force that the model I2 can apply to the radula/odontophore after 8 s of maximal stimulation (dashed line labeled "I2 force") is calculated by multiplying **a** times **b** times the maximum force in I2 (F_{oI2}) and compared to the opposing passive forces generated by the hinge (**c**, *solid line*). The hinge force's upper and lower bounds (*gray shading*), as well as projected physiological forces (*central solid line*), are indicated. The upper bound of the hinge force is at a radula/odontophore velocity of 1.1×10^{-2} m/s, which is 250% faster than velocities observed in vivo. The central line is at a radula/odontophore velocity of 4.0×10^{-3} m/s, the maximum radula/odontophore velocity observed during swallowing from Neustadter et al. (2002). The lower bound is the steady-state passive hinge forces. At displacements of less than 0.45 BML, the maximal I2 force is greater than the resistive hinge force. Thus, the I2 is strong enough to protract the radula/odontophore to these displacements. At larger displacements, however, the model I2 is insufficiently strong to overcome the hinge forces and protract the radula/odontophore. Some additional mechanism would be required to protract the radula/odontophore to the displacements observed in biting. **d** Length/tension of I1/I3. **e** I1/I3's mechanical advantage changes sign as the radula/odontophore protracts (at the transition point marked "Trans."). **f** Initially, the curve follows the I2 force curve in Fig. 4c. After the radula/odontophore has protracted by 0.25 BML, the values in **d** and **e** are multiplied together and by the maximum I1/I3 force (F_{oI3}) and added to the I2 force curve in Fig. 4c. If the model I1/I3 is cocontracted with I2, I1/I3 can add enough force to protract the radula/odontophore to a biting displacement (**c**; *solid line* labeled I2 + I1/I3 force)

$T_{I1/I3}$) and the angle between I1/I3 and I2 (ϕ , Fig. 1d), both muscles' geometry were integrated about the model's axis of symmetry:

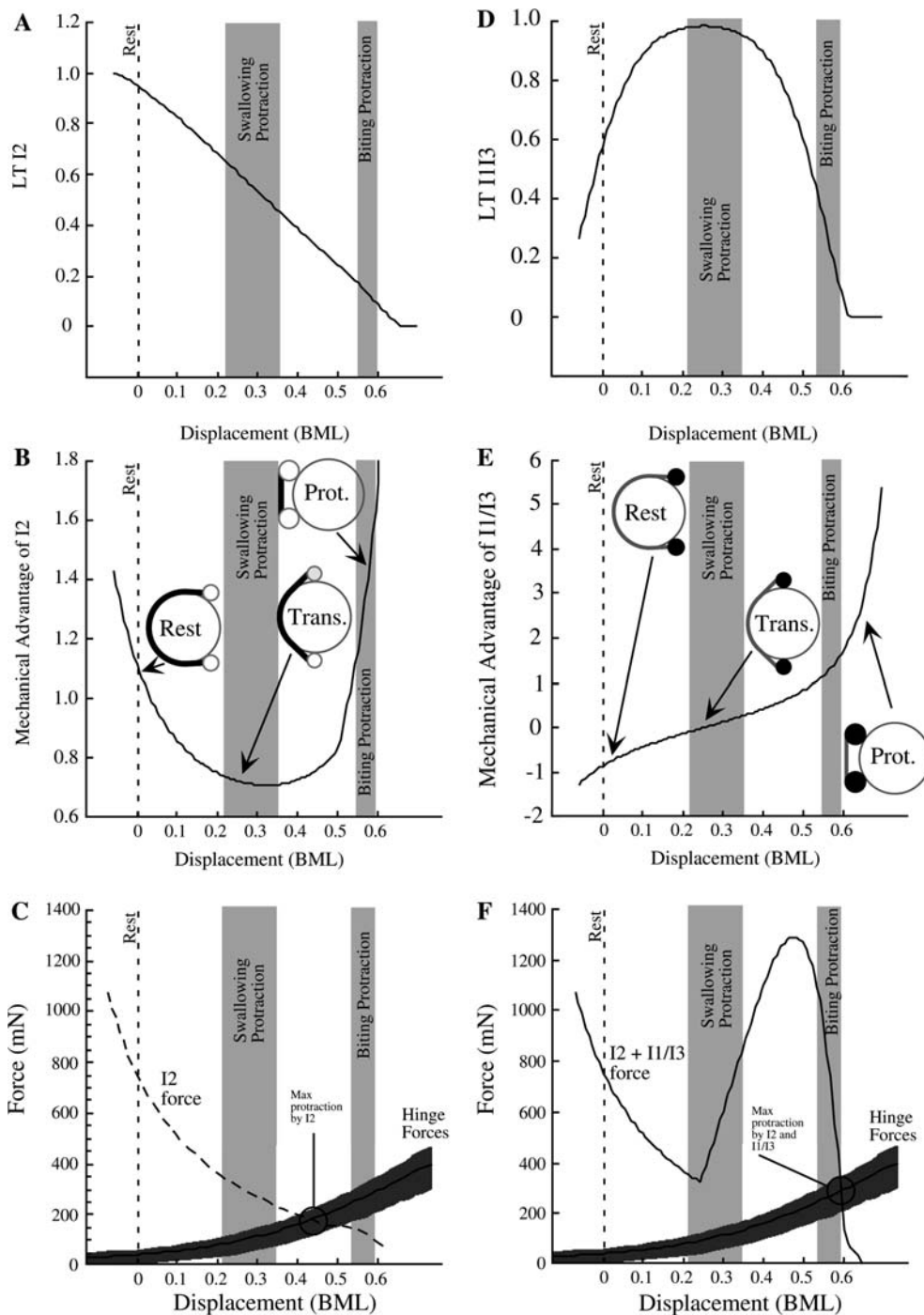
$$F_1 = \int_0^{2\pi} T_{I2} \cos(\phi) d\gamma + \text{Hingeforce}, \quad (11a)$$

$$F_2 = \int_0^{2\pi} (T_{I2} \sin(\phi) + T_{I1/I3}) d\gamma. \quad (11b)$$

Hingeforce is the force in the hinge defined by the model described in Sutton et al. (2004).

2.8 Conversion of ENG and EMG into muscle input frequency

The I2 EMG and the buccal nerve 2 ENG were incorporated into the model in different ways. The I2 EMG was rectified and scaled by a constant [using the same process used in Yu et al. (1999) but with a different scaling factor, given in Table 1]. Buccal nerve 2 ENG was converted to frequency by using a windowing algorithm to divide the ENG into three categories: small extracellular potentials, medium-sized potentials, and large potentials, corresponding to different groups of motor neurons (Morton



and Chiel 1993a). The largest reciprocal of each interspike interval was passed into the activation function.

3 Results

To test the hypothesis that neural control may alter the phase of activation of the context-dependent I3 muscle as the forces in the protractor I2 muscle fall, we first used the model to predict the maximum force that I2 could apply to the radula/odontophore at different displacements. We compared this force to the opposing steady-

state force of the hinge. We used these results to predict the maximum possible displacement of the radula/odontophore that could be caused by I2 alone and compared that prediction to in vivo radula/odontophore displacements during swallowing and biting. Finally, to test how neural control may compensate for the decreasing mechanical advantage of I2 during biting as opposed to swallowing, we used in vivo neural recordings from biting and swallowing behaviors as input to the model.

The maximum anterior force that the model I2 can apply to the radula/odontophore decreases as the radula/odontophore protracts. There are two mechanisms

for this reduction: I2's length–tension property (Fig. 4a) and I2's mechanical advantage on the radula/odontophore (Fig. 4b). Protraction of the radula/odontophore causes the model I2 to shorten and descend along its length–tension curve, greatly reducing I2's ability to generate tension. In addition, as the radula/odontophore protracts, the changing geometry of the model I2 causes tension in I2 to result in less net force on the radula/odontophore, making the I2 less able to protract the radula/odontophore [Fig. 4b, (equation 11a)]. Once the I3 is positioned on the posterior half of the radula/odontophore, however, the attachment between I2 and I1/I3 allows the model I2 to close the jaws behind the radula/odontophore (see Fig. 4b, sketch labeled “Prot.”). This jaw closure further pushes the radula/odontophore forward, increasing I2's mechanical advantage. Multiplying the I2's length–tension and mechanical advantage by the maximum tension generated by I2 after 8 s of maximal activation (i.e., an input frequency of 20 Hz) yields the maximum resultant force on the radula/odontophore that the model I2 can generate as a function of position (Fig. 4c).

As the radula/odontophore protracts, the hinge force resisting protraction increases (Fig. 4c). The stiffness of both the elastic and the viscoelastic components of the hinge increase at larger displacements, greatly increasing the resistance to further protraction. The hinge force is nonlinear because the model includes both dynamic and static elastic components (Sutton et al. 2004).

The model I2 is strong enough to protract the radula/odontophore to maximal swallowing displacements but not to maximal biting displacements. The model I2's maximal force exceeds the resistive force of the hinge as it protracts the radula/odontophore to about 0.45 Buccal Mass Lengths (BML; Fig. 4c). Thus I2 can protract the radula/odontophore to the displacement observed in swallowing (0.28 ± 0.07 BML; data from Neustadter et al. 2002; Fig. 4c, middle gray bar). At displacements greater than 0.45 BML, however, the hinge force exceeds the model I2's maximal resultant force, and thus the model suggests that I2 is too weak to protract the radula/odontophore to the magnitudes seen in biting [0.56 ± 0.02 BML; data from Sutton et al. (2004); Fig. 4c, rightmost gray bar].

The model suggests two possible mechanisms that the buccal mass could use in addition to contraction of I2 to protract the radula/odontophore to a biting displacement: (i) I1/I3 could be activated during protraction, and (ii) I2 could be neuromodulated to increase its strength.

To protract the radula/odontophore to a biting displacement, I1/I3 could be activated. As the radula/odontophore protracts, I1/I3's mechanical advantage changes, so that instead of acting as a radula/odontophore retractor, it acts as a radula/odontophore protractor (Fig. 4e; I1/I3's ability to retract or protract are shown by the inset schematic diagrams). Thus, the model suggests the hypothesis that I1/I3's function could be context dependent. If I1/I3 were contracted while the radula/odontophore was displaced anteriorly, the additional force on the radula/odontophore could be large enough to protract the odontophore farther to a biting displacement (Fig. 4f).

To protract the radula/odontophore to a biting displacement, I2 could also be neuromodulated by application of serotonin or myomodulin (Hurwitz et al. 2000). Neuromodulators may change the maximum contractile force as well as alter the rate of contraction. If I2's maximum contractile force, F_{oI2} , were tripled by a neuromodulator, I2 would be sufficiently strong to protract the radula/odontophore to a biting displacement (Fig. 5, black line labeled “A”). However, if neuromodulation only increased I2's rate of contraction, I2 would still not be strong enough to produce the maximum displacement observed during biting (Fig. 5, gray line labeled “B”).

How could neural control exploit the context dependence of I1/I3 to compensate for the falling mechanical advantage of protractor muscle I2? Using input based on in vivo electromyographic and electroneurographic recordings of I2 and I1/I3 (six swallows and nine bites; Hurwitz et al. 1996), the model predicts that, during biting, the timing of onset of I1/I3 activity will enable it to assist I2 in protracting the radula/odontophore. First, the model predicts radula/odontophore displacements in both swallowing and biting that are consistent with what is measured from in vivo MRI (an example bite and swallow are shown in Fig. 6 A, B). Second, during most of the swallowing behaviors (five out of six), I2 was used to protract the radula/odontophore and I1/I3 was used to retract the radula/odontophore. In the sixth behavior, I2 had protracted the radula/odontophore far enough for I1/I3 to further protract the radula/odontophore when I1/I3 was activated. Third, during most of the biting behaviors (seven out of nine), the model demonstrated that the earlier

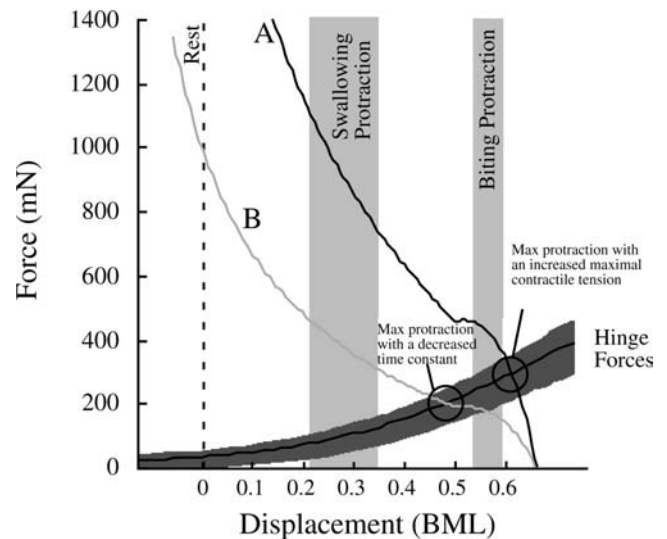


Fig. 5. Possible effects of neuromodulation on the force that the model I2 could apply to the radula/odontophore. If neuromodulation triples I2's maximal contractile tension (black line labeled “A”), I2 would be strong enough to protract the radula/odontophore to a biting displacement. If neuromodulation instead decreased the time constant of activation without affecting the maximal contractile tension (gray line labeled “B”), I2 would still be insufficiently strong to protract the radula/odontophore to a biting displacement

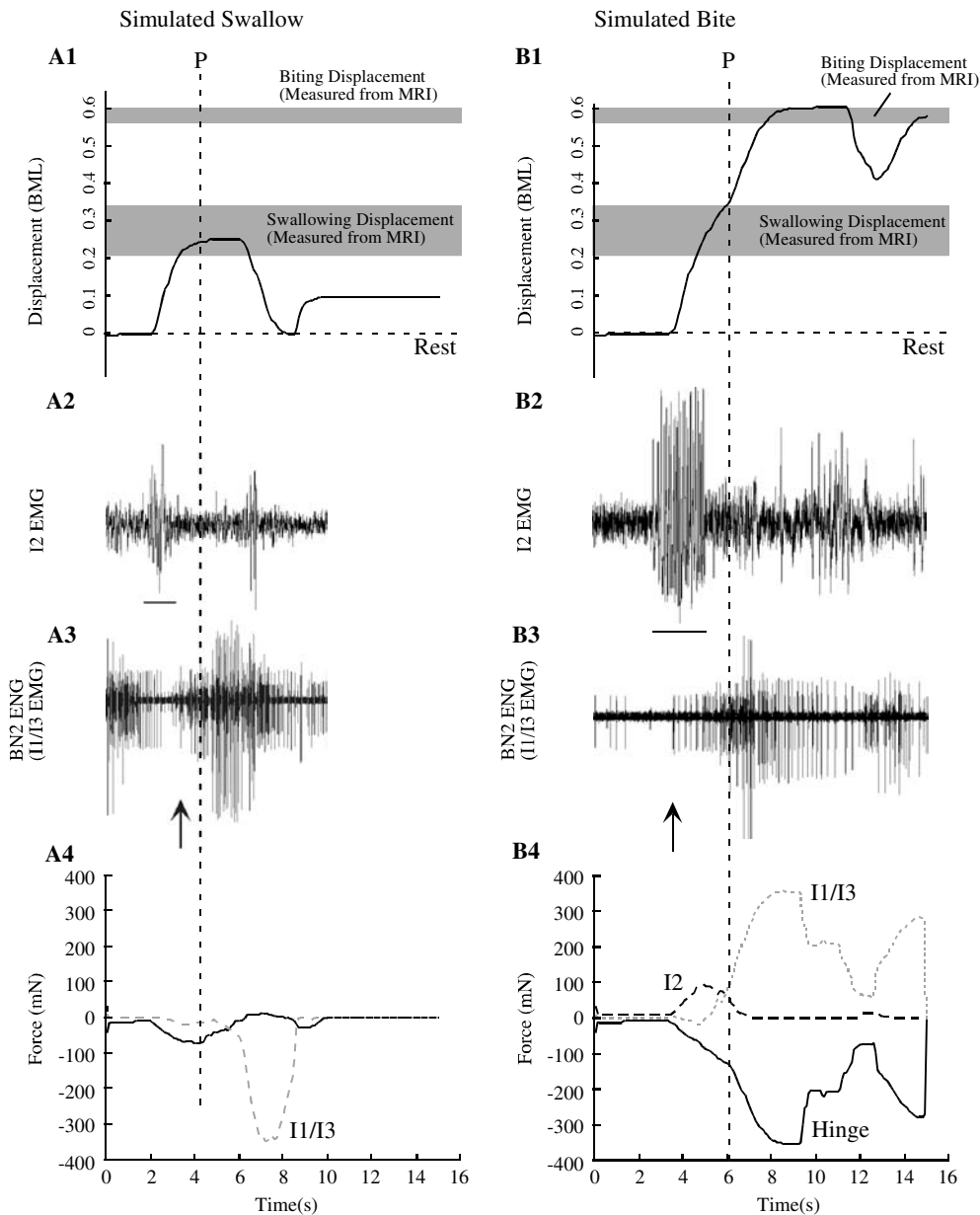


Fig. 6a1–a4, b1–b4. Model response to the input of in vivo biting and swallowing I2 electromyograms (EMG) and buccal nerve 2 electro-neurogram [BN2 ENG; neural recordings from Hurwitz et al. 1996; note that BN2 innervates the I1/I3 muscles]. During both behaviors, the model predicts radula/odontophore protraction magnitudes that match in vivo MRI measurements. The time of peak protraction for the in vivo behaviors are marked by the *dashed gray lines* marked “P.” Throughout swallowing (**a1**), the model predicts that I1/I3 will act to retract the radula/odontophore (I1/I3’s force is negative, **a4** – *dashed gray line*). Throughout biting (**b1**), the model predicts that I1/I3 will protract the radula/odontophore (I1/I3’s force is positive,

b4 – *dashed gray line*). Note that the onset of large unit activity in the nerve innervating I1/I3 is earlier in biting than in swallowing (*arrows* under second trace) relative to the time of activation of I2 during protraction (*line* under first trace). This change in onset of I1/I3 activity was consistently observed in all bites ($N = 9$) and swallows ($N = 6$) that were studied. During both behaviors, the I2 force (**a4, b4** – *dashed black line*) protracts the radula/odontophore, and the hinge force (**a4, b4** *solid black line*) opposes radula/odontophore protraction. The model does not duplicate the timing of peak protraction of the in vivo behavior due to model simplifications

activation of I1/I3 relative to the activation of I2 allowed I1/I3 to assist I2 in further protracting the radula/odontophore. The other two biting behaviors activated I1/I3 before the radula/odontophore had protracted far enough for I1/I3 to become a protractor. By activating I1/I3 earlier in biting behaviors, neural control can compensate for the weakening mechanical advantage of I2 by activating I1/I3 to assist radula/odontophore protraction.

4 Discussion

As the radula/odontophore moves anteriorly, the anteriorly directed force that I2 can apply is reduced by both I2’s length–tension property and I2’s mechanical advantage. The hinge force that resists radula/odontophore anterior motion increases as the radula/odontophore protracts. This allows the model I2 alone to protract the radula/

odontophore by no more than 0.45 BML; the passive hinge force is too large to allow larger protractions. The model I2 is incapable of protracting the radula/odontophore to a full biting protraction (0.56 BML). If I1/I3 were activated, or I2 were sufficiently neuromodulated, however, the buccal mass would be able to protract the radula/odontophore to a biting displacement. Activating the model with in vivo neural and muscular activations observed during bites predicts that I1/I3 will act to protract the radula/odontophore.

Assumptions of the kinetic model cause it to differ from the in vivo buccal mass. We will address each of these differences in turn: (1) the in vivo I2 is not a uniform sheet, (2) the I2 is stimulated less in vivo than in the model simulation, (3) the in vivo I2 cannot close the I1/I3, (4) the model's rest position may differ from the in vivo rest position, and (5) the hinge can generate active as well as passive forces. We will argue that these assumptions do not invalidate conclusions about the limitations of I2's protraction ability. In addition, there are differences between model representations of I1/I3 and of neuromodulation's effect on I2: (6) the in vivo I1/I3 is a continuous sheet, and not a torus, and (7) the quantitative effect of neuromodulation on I2 is not known. We will also discuss these assumptions.

The assumption that I2 is a hemispherical sheet may overestimate I2's strength. The in vivo I2 curves around the posterior surface of the radula/odontophore and splits into two bands (Drushel et al. 1998; Yu et al. 1999). Not being affixed all the way around the posterior side of the buccal mass would make the in vivo I2 weaker than the model I2. If the in vivo I2 were weaker than the model I2, however, it would strengthen the hypothesis that, in vivo, I2 is insufficiently strong to displace the radula/odontophore anteriorly to a biting displacement.

The long I2 activation time (8 s) overestimates I2's strength. In vivo, the animal completes a biting behavior in under 7 s (Susswein et al. 1976; Rosen et al. 1983, 1989), with the I2 only receiving stimulation for between half to two thirds of that time (Hurwitz et al. 1996), suggesting that, in vivo, the I2 is stimulated for a maximum of 5–6 s. This would cause the model to overestimate I2's activation by 20–30% (Yu et al. 1999) and thus cause it to overestimate I2's strength. This overestimate, however, would also strengthen our hypothesis.

The assumption that, as I2 fully shortens, it can close I1/I3 and further protract the radula/odontophore (Fig. 4b, diagram labeled "Prot.") also overestimates I2's mechanical advantage. In vivo, most of I2's muscle fibers run dorsoventrally. The I1/I3/jaw complex, however, opens mediolaterally, which would prevent I2 contraction from closing the jaws. If I2 is not able to close the jaws, the mechanical advantage of I2 is about half of what the model predicts (data not shown), and I2 is less able to protract the radula/odontophore.

It is possible that the model's rest position is not equivalent to the physiological rest position. The model rest position is the position where the hinge, I2, and I1/I3 are at static equilibrium. At the rest displacement, the model's predicted I2 length is 95% of I2's optimal length; in vivo, I2's rest length is 85% of I2's optimal length (Yu et al.

1999). The model overestimates I2's rest length, overestimates I2's length–tension parameter, and thus overestimates I2's strength, again supporting our hypothesis.

Finally, the hinge can generate active as well as passive forces (Sutton et al. 2004, Fig. 10) that oppose protraction. Thus, the model underestimates the total force opposing I2 during protraction. This strengthens our hypothesis.

In summary, differences between the model and the in vivo buccal mass do not invalidate the hypothesis about I2. The differences all cause the model to overestimate I2's relative strength compared to the hinge forces. Thus, the model represents an upper bound on the ability of I2 to protract the radula/odontophore.

Our analysis of I1/I3's mechanical advantage focuses on its posterior portion. If the I1/I3 is modeled as a continuous sheet with uniform activation, the mechanical advantage of I1/I3 will still be dependent on radula/odontophore position relative to the net force in I1/I3: if the radula/odontophore is posterior to the net force in I1/I3, I1/I3 will act as a retractor; if the radula/odontophore is anterior to the net force in I1/I3, I1/I3 will act as a protractor (data not shown). Alternatively, if the posterior portion of I1/I3 exerts more force than its anterior portion, the net effect of I1/I3 will still depend on the position of the net force relative to the midline of the radula/odontophore. There is in vivo evidence that the posterior portion of I1/I3 may be differentially activated. A neuron that innervates the posterior and medial portions of the I1/I3/jaw complex (Church and Lloyd 1994) appears to become active earliest during the onset of activity in the pool of motor neurons that innervates the I1/I3/jaw complex (Morton and Chiel 1993a), so that the posterior portion may be activated earlier than the anterior portion of the I1/I3/jaw complex.

While the exact effect of neuromodulation on I2's muscle force is unknown, previous studies suggest that neuromodulation decreases I2's time constant of activation. It is known that serotonin is an in vivo *Aplysia* neuromodulator (Weiss et al. 1978) that increases the magnitude of I2 contractions (Hurwitz et al. 2000). However, previous studies did not determine whether neuromodulation increased the maximal muscle contractile force, or whether it decreased the time constant of muscle activation, because I2's maximal contractile force was not measured (Brezina et al. 2000b). If I2's activation time constant was decreased, but the maximal contractile force was unchanged, I2 would still have insufficient strength to protract the radula/odontophore to a biting displacement (Fig. 5, gray line labeled 'B'). It is known, however, that lesioning a serotonergic neuron, the MCC, does not decrease a bite's protraction magnitude, but does increase the time required to bite (Rosen et al. 1983, 1989). This result suggests that serotonin decreases the muscle's time constant, but may not be critical for producing the magnitude of protraction seen in biting.

Throughout the biting simulations, the I1/I3 protracts the radula/odontophore. This evidence, however, is not conclusive, because I1/I3's contractile dynamics are estimated from measurements made on I2. In addition, neuromodulation is not modeled. The two bites that did not use I1/I3 as a protractor failed to produce meaningful

behavior because of premature activation of I1/I3 (data not shown). This is probably because the model assumed that every BN2 action potential was excitatory. It is known that one of I1/I3's motor neurons, B47, is an inhibitory neuron (Church et al. 1993) that fires during the protraction phase of ingestive behaviors (Church and Lloyd 1994). Our simulation, however, did not differentiate B47 potentials from potentials generated by excitatory neurons, which may have caused the model to overstimulate I1/I3 during protraction. In turn, this may have caused the model to fail in two of the nine bites. Also, the posterior section of I1/I3 (innervated by B10, B4, and B5) may be activated at a different time than the anterior section (innervated by B3 and B38; Church and Lloyd 1994). This differential innervation may play a role in I1/I3's function during biting and swallowing behaviors. In order to accurately predict whether I1/I3 is acting as a radula/odontophore protractor *in vivo*, EMG recordings from I1/I3 that differentiated between motor neuron activities would have to be combined with an accurate model of I1/I3's contractile dynamics. This would allow us not only to analyze the role of I1/I3 in behavior, but also to look at the functional roles of the individual motor neurons that innervate I1/I3.

Biomechanics determines when muscle activations will cause large changes in behavior and when they will not. For example, at rest, nervous stimulation of I2 will cause large motions of the radula/odontophore to the jaws, with larger stimulations of the I2 generating larger motions. If the radula/odontophore is protracted, however, the system is insensitive to increased stimulation of I2 because both mechanical advantage and length–tension properties are acting to reduce resultant I2 force on the radula/odontophore. Thus the relative importance of an increment in I2 activation on behavior is dependent on the initial radula/odontophore position.

What control implications do these biomechanics have for the generation of behaviors? At rest, the passive forces within the buccal mass create a zone of neutral stability (Fig. 7: no muscles active; see also Fig. 6 in Sutton et al. 2004). Activation of I2 creates a stable equilibrium point, with larger activations of I2 moving this stable equilibrium point farther from rest to a maximum of 0.45 BML from rest (Fig. 7: I2 maximally active). Because of the biomechanics of I1/I3, activation of I1/I3 creates an unstable equilibrium point and two stable equilibrium points, one in peak protraction and one in peak retraction (Fig. 7: I1/I3 maximally active). By changing I2 activation, the nervous system can mediate where the radula/odontophore is relative to the unstable equilibrium point in order to use I1/I3 to generate either large protractions or large retractions. In the swallowing simulations, the nervous system activated I1/I3 while the radula/odontophore was displaced below the location of the unstable equilibrium point, so that I1/I3 moved the radula/odontophore to the stable equilibrium point at which it was stably retracted by I1/I3 (Fig. 6). In the biting simulations, the nervous system activated I1/I3 after the radula/odontophore passed the location of the unstable equilibrium point, so that the I1/I3 moved

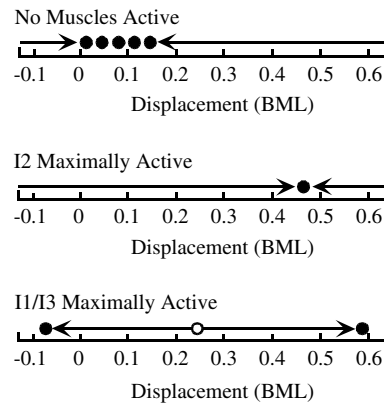


Fig. 7a,b. Phase portrait of the model under the conditions of **a** no active muscles, **b** I2 maximally active, and **c** I1/I3 maximally active. Stable equilibria are marked with filled circles, and unstable equilibria are marked with open circles. When the system is at rest, the radula/odontophore sits in a zone of neutral stability (A, Sutton et al. 2004). Contraction of I2 protracts the radula/odontophore to the jaws (b). Subsequent contraction of I1/I3, however, creates an unstable equilibrium point that either greatly protracts or retracts the radula/odontophore, depending on the radula/odontophore's initial position before the contraction (Fig. 4e). By manipulating the initial position of the radula/odontophore relative to this unstable equilibrium point, the *Aplysia* nervous system appears to control the actions of I1/I3 on the radula/odontophore

the radula/odontophore to the stable equilibrium point at which it was stably protracted by I1/I3 (Fig. 6). Manipulation of the equilibrium points may be the control strategy that the *Aplysia* nervous system uses to generate biting and swallowing. This is very similar to the equilibrium point hypothesis control strategy that has been proposed for vertebrates (Bizzi et al. 1992; Flash and Sejnowski 2001).

Controlling the location of the unstable equilibrium point represents another opportunity for the nervous system to control the effects of I1/I3 on the radula/odontophore. Changing the shape of the radula/odontophore, and thus the location of the widest part of the radula/odontophore relative to the center of I1/I3, could change the location of the unstable equilibrium point and place I1/I3 in the basin of attraction of a different stable equilibrium point, even if the relative positions of I1/I3 and the radula/odontophore have not changed. In particular, at the peak of protraction of biting, closing the halves of the radula/odontophore might change the position of the unstable equilibrium point, so that steady activation of I1/I3 initially assists protraction and then, after the shape change, helps to initiate retraction.

Acknowledgements. The authors would like to thank Dr. Joseph Mansour for his help with data analysis and his comments on an earlier draft of the manuscript. We would also like to thank Dr. Richard Drushel for his anatomical illustrations of the buccal mass (Fig. 1). This work was supported by NSF Grants IBN9974394 and IBN0218386, NSF IGERT Grant 345-1898, and HHMI Grant 71199600606.

References

- Abbott BC, Baskin RJ (1962) Volume changes in frog muscle during contraction. *J Physiol* 161:379–391
- Alfaro ME, Herrel A (2001) Introduction: major issues of feeding motor control in vertebrates. *Am Zool* 41:1243–1247
- Belanger JH, Orchard I (1993) The locust ovipositor opener muscle: properties of the neuromuscular system. *J Exp Biol* 174:321–342
- Bizzi E, Hogan N, Mussa-Ivaldi FA, Giszter S (1992) Does the nervous system use equilibrium-point control to guide single and multiple joint movements? *Behav Brain Sci* 15(4):603–613
- Brezina V, Orekhova IV, Weiss KR (2000a) The neuromuscular transform: the dynamic, nonlinear link between motor neuron firing patterns and muscle contraction in rhythmic behaviors. *J Neurophysiol* 83:207–231
- Brezina V, Orekhova IV, Weiss KR (2000b) Optimization of rhythmic behaviors by modulation of the neuromuscular transform. *J Neurophysiol* 83:260–279
- Buneo CA, Soechting JF, Flanders M (1997) Postural dependence of muscle actions: implications for neural control. *J Neurosci* 17(6):2128–2142
- Chiel HJ, Crago PE, Mansour JM, Hathi K (1992) Biomechanics of a muscular hydrostat: a model of lapping by a reptilian tongue. *Biol Cybern* 67:403–415
- Chiel HJ, Neustadter DM, Herman RL, Sutton GP, Drushel RF (2003) Kinematics of biting in *Aplysia* suggest that jaw muscle function may be context dependent. *Soc Neurosci Abstr* 606.12
- Church PJ, Cohen KP, Scott ML, Kirk MD (1991) Peptidergic motoneurons in the buccal ganglia of *Aplysia californica*-immunocytochemical, morphological, and physiological characterizations. *J Comp Physiol A* 168(3):323–336
- Church PJ, Whim MD, Lloyd PE (1993) Modulation of neuromuscular transmission by conventional and peptide transmitters released from excitatory and inhibitory motor neurons in *Aplysia*. *J Neurosci* 13(7):2790–2800
- Church PJ, Lloyd PE (1994) Activity of multiple identified motor neurons recorded intracellularly during evoked feeding-like motor programs in *Aplysia*. *J Neurophysiol* 72(4):1794–1809
- Drushel RF, Neustadter DM, Shallenberger LL, Crago PE, Chiel HJ (1997) The kinematics of swallowing in the buccal mass of *Aplysia californica*. *J Exp Biol* 200:735–752
- Drushel RF, Neustadter DM, Hurwitz I, Crago PE, Chiel HJ (1998) Kinematic models of the buccal mass of *Aplysia californica*. *J Exp Biol* 201:1563–1583
- Evans CG, Rosen SC, Kupfermann I, Weiss KR, Cropper EC (1996) Characterization of a radula opener neuromuscular system in *Aplysia*. *J Neurophysiol* 76(2):1267–1281
- Evans CG, Cropper EC (1998) Proprioceptive input to feeding motor programs in *Aplysia*. *J Neurosci* 18(19):8016–8031
- Flash T, Sejnowski TJ (2001) Computational approaches to motor control. *Curr Opin Neurobiol* 11:655–662
- Fox LE, Lloyd PE (1997) Serotonin and the small cardioactive peptides differentially modulate two motor neurons that innervate the same muscle fibers in *Aplysia*. *J Neurosci* 17(16):6064–6074
- Howells HH (1942) The structure and function of the alimentary canal of *Aplysia punctata*. *Q J Microscop Sci* 83:357–397
- Hoy MG, Zajac FE, Gordon ME (1990) A musculoskeletal model of the human lower extremity: the effect of muscle, tendon and moment arm on the moment-angle relationship of musculotendon actuators at the hip, knee, and ankle. *J Biomech* 23:157–169
- Hurwitz I, Neustadter DM, Morton DW, Chiel HJ, Susswein AJ (1996) Activity patterns of the B31/B32 pattern initiators innervating the I2 muscle of the buccal mass during normal feeding movements in *Aplysia californica*. *J Neurophysiol* 75(4):1309–1326
- Hurwitz I, Kupfermann I, Susswein AJ (1997) Different roles of neurons B63 and B34 that are active during the protraction phase of buccal motor programs in *Aplysia californica*. *J Neurophysiol* 78(3):1305–1319
- Hurwitz I, Cropper EC, Vilim FS, Alexeeva V, Susswein AJ, Kupfermann I, Weiss KR (2000) Serotonergic and peptidergic modulation of the buccal mass protractor muscle (I2) in *Aplysia*. *J Neurophysiol* 84:2810–2820
- Ijspeert AJ (2001) A connectionist central pattern generator for the aquatic and terrestrial gaits of a simulated salamander. *Biol Cybern* 84:331–348
- Jing J, Weiss KR (2001) Neural mechanisms of motor program switching in *Aplysia*. *J Neurosci* 21(18):7349–7362
- Jing J, Weiss KR (2002) Interneuronal basis of the generation of related but distinct motor programs in *Aplysia*: implications for current neuronal models of vertebrate intralimb coordination. *J Neurosci* 22(14):6228–6238
- Jing J, Vilim FS, Wu JS, Park JH, Weiss KR (2003) Concerted GABAergic actions of *Aplysia* feeding interneurons in motor program specification. *J Neurosci* 23(12):5283–5294
- Kupfermann I (1974) Feeding behavior in *Aplysia*: a simple system for the study of motivation. *Behav Biol* 10:1–26
- Kargo WJ, Rome LC (2002) Functional morphology of proximal hindlimb muscles in the frog *Rana pipiens*. *J Exp Biol* 205:1987–2004
- Kaske A, Winberg G, Coster J (2003) Traveling-wave pattern generator controls movement and organization of sensory feedback in a spinal cord model. *Biol Cybern* 88:11–19
- Koike Y, Kawato M (1995) Estimation of dynamic joint torque and trajectory formation from surface electromyograph signal using a neural network model. *Biol Cybern* 73:291–300
- Lotshaw DP, Lloyd PE (1990) Peptidergic and serotonergic facilitation of a neuromuscular synapse in *Aplysia*. *Brain Res* 526:81–94
- Miller MW, Rosen SC, Schissel SL, Cropper EC, Kupfermann I, Weiss KR (1994) A population of SCP-containing neurons in the buccal ganglion of *Aplysia* are radula mechanoreceptors and receive excitation of central origin. *J Neurosci* 14(11):7008–7023
- Morton DW, Chiel HJ (1993a) The timing of activity in motor neurons that produce radula movements distinguishes ingestion from rejection in *Aplysia*. *J Comp Physiol A* 173(5):519–536
- Morton DW, Chiel HJ (1993b) *In vivo* buccal nerve activity that distinguishes ingestion from rejection can be used to predict behavioral transitions in *Aplysia*. *J Comp Physiol A* 172(1):17–32
- Neustadter DM, Drushel RF, Chiel HJ (2002) Kinematics of the buccal mass during swallowing based on magnetic resonance imaging in intact, behaving *Aplysia californica*. *J Exp Biol* 205:939–958

- Rosen SC, Weiss KR, Cohen JL, Kupfermann I (1982) Inter-ganglionic cerebral-buccal mechanoafferents of *Aplysia*-receptive fields and synaptic connections to different classes of neurons involved in feeding behavior. *J Neurophysiol* 48(1):271–288
- Rosen SC, Kupfermann I, Goldstein RS, Weiss KR (1983) Lesion of a serotonergic modulatory neuron in *Aplysia* produces a specific defect in feeding behavior. *Brain Res* 260:151–155
- Rosen SC, Weiss KR, Goldstein RS, Kupfermann I (1989) The role of modulatory neuron in feeding and satiation in *Aplysia*: effects of lesioning of the serotonergic metacerebral cells. *J Neurosci* 9(5):1562–1578
- Rosen SC, Miller MW, Cropper EC, Kupfermann I (2000a) Outputs of radula mechanoafferent neurons in *Aplysia* are modulated by motor neurons, interneurons, and sensory neurons. *J Neurophysiol* 83(3):1621–1636
- Rosen SC, Miller MW, Evans CG, Cropper EC, Kupfermann I (2000b) Diverse synaptic connections between peptidergic radula mechanoafferent neurons and neurons in the feeding system of *Aplysia*. *J Neurophysiol* 83(3):1605–1620
- Susswein AJ, Kupfermann I, Weiss KR (1976) The stimulus control of biting in *Aplysia*. *J Comp Physiol* 108:75–96
- Sutton GP, Mackinn JB, Gartman SS, Sunny GP, Beer RD, Crago PE, Chiel HJ (2004) Passive properties within the feeding apparatus of *Aplysia* aid retraction in biting but not in swallowing. *J Comp Physiol A* 190:501–514
- Taga G (1995) A model of the neuro-musculo-skeletal system for human locomotion. I. Emergence of basic gait. *Biol Cybern* 73: 97–111
- Van Leeuwen JL, Kier WM (1997) Functional design of tentacles in squid: linking sarcomere ultrastructure to gross morphological dynamics. *Philos Trans R Soc Lond B* 352:551–571
- Van Leeuwen JL, De Groot JH, Kier WM (2000) Evolutionary mechanics of protrusible tentacles and tongues. *Neth J Zool* 50(2):113–139
- Weiss KR, Cohen JL, Kupfermann I (1978) Modulatory control of buccal musculature by a serotonergic neuron (metacerebral cell) in *Aplysia*. *J Neurosci* 41(1):181–203
- Yoshida N, Domen K, Koike Y, Kawato M (2002) A method for estimating torque-vector directions of shoulder muscles using surface EMGs. *Biol Cybern* 86:167–177
- Yu SN, Crago PE, Chiel HJ (1999) Biomechanical properties and a kinetic simulation model of the smooth muscle I2 in the buccal mass of *Aplysia*. *Biol Cybern* 81:505–513
- Zajac FE (1993) Muscle coordination of movement: a perspective. *J Biomech* 26:109–124.
- Zajac FE, Neptune RR, Kautz SA (2002) Biomechanics and muscle coordination of human walking, Part I: introduction to concepts, power transfer, dynamics and simulations. *Gait Posture* 16: 215–232